A new neutrino source for the study of the solar neutrino physics in the vacuum-matter transition region

Jae Won Shin and Myung-Ki Cheoun*

Department of Physics, Soongsil University, Seoul 156-743, Korea

(Dated: Jan. 4, 2016)

Production of a neutrino source through proton induced reaction is studied by using the particle transport code, GEANT4. Unstable isotope such as ^{27}Si can be produced when ^{27}Al target is bombarded by 15 MeV energetic proton beams. Through the beta decay process of the unstable isotope, a new electron-neutrino source in the $1.0 \sim 5.0$ MeV energy range is obtained. Proton induced reactions are simulated with JENDL High Energy File 2007 (JENDL/HE-2007) data and other nuclear data. For radioactive decay processes, we use "G4RadioactiveDecay" model based on the Evaluated Nuclear Structure Data File (ENSDF). We suggest target systems required for future's solar neutrino experiments, in particular, for the vacuum-matter transition region. As for the detection system of the new neutrino source, we evaluate reaction rates for available radiochemical detectors and LENA type scintillator detector. Possibility of detecting sterile neutrinos is also discussed.

PACS numbers: 26.65.+t, 14.60.Pq, 24.10.Lx, 02.70.Uu

Keywords: neutrino source, vacuum-matter transition region, solar physics, GEANT4, JENDL/HE-2007, ENSDF

I. INTRODUCTION

The neutrino oscillation mechanism which was firstly suggested by Pontecorvo [1–5] plays important roles to explain the discrepancies among the measured solar neutrino flux and/or the theoretical one, so-called solar neutrino problem. Since the first observation of the effects of neutrino oscillation was done in Homestake Experiments [6], many experiments, such as

*Electronic address: cheoun@ssu.ac.kr

KamioKanDe [7] and SNO [8] facilities, had confirmed the neutrino oscillation through more refined and advanced detection.

In addition to the oscillation in vacuum, the recent experimental data at Borexino [9], which measured *pep* neutrino in $1.0 \sim 1.5$ MeV, point out to need to consider Mikheyev-Smirnov-Wolfenstein (MSW) [10–13] large mixing angle (LMA) solutions. The MSW model predicts a transition from vacuum-dominated to matter-enhanced oscillations relevant to the metallicity problem in the solar model, but experimental understanding is still insufficient in this energy region.

One of the future open issues related to the vacuum-matter transition region in the solar neutrino physics is the determination of the electron-neutrino survival probability $\mathrm{P}(\nu_e \rightarrow \nu_e)$ in that region [14], which is also closely related to questions such as existence of sterile neutrinos [15, 16] and/or the non-standard neutrino interactions (NSI) [17], roles of CNO cycle in the Sun (metallicity problem) [18, 19], etc.

For this reason, it becomes of importance to detect in detail the solar neutrino in the transition region. Moreover, it would be more efficient if we have the controllable neutrino source in the energy region, which may enable us to extract both the total number and the energy distribution of neutrinos in a more accurate way, with the more elaborate detection system. In this work, we propose an accelerator based new artificial electron-neutrino source for the experiments of the vacuum-matter transition region. By adjusting the incident proton energy, we can produce a specific unstable isotope as an efficient electron-neutrino source. Unstable isotope, ^{27}Si, is our main neutrino source, which can be produced through $^{27}\mathrm{Al(p,n)}^{27}\mathrm{Si}$ reaction and emits electron-neutrinos through radioactive decay processes. In this case, the neutrinos can have the energy similar to the transition region.

We outline the paper in the following way. In Sec. II, we summarize the simulation method used in this work. Benchmarking simulations for $^{27}\mathrm{Al(p,n)}^{27}\mathrm{Si}$ reaction, calculations for ^{27}Si yields and energy spectra of electron-neutrinos from decay of ^{27}Si are presented in Sec. III. Electron-neutrino detections, event rate of the scattered electron and possibility of detecting the sterile neutrino are discussed in Sec. IV and V, respectively. The summary is given in Sec. VI.

II. SIMULATION METHOD

As an electron-neutrino source, we consider ^{27}Si isotope in this work, which can be produced through ^{27}Al(p,n)^{27}Si reaction with a threshold energy E_{th} of 5.803 MeV. To evaluate ^{27}Si yields produced by proton beams on ^{27}Al target, we use the particle transport code, GEANT4 (GEometry ANd Tracking) v10.1 [20, 21], which is a tool kit that allows for microscopic Monte Carlo simulations of particles interacting with materials.

For proton inelastic scattering, four different hadronic models such as "G4BertiniCascade" [22], "G4BinaryCascade" [23], "G4Precompound" [24] and "G4INCLCascade" [25] are available in GEANT4 (v10.1). To check the validity of the models, we first perform simulations of ^{27}Si production by p + ^{27}Al reaction and compare the calculated results with the experimental data taken from the EXFOR database [26]. For brevity, we refer to GEANT4 simulations with "G4BertiniCascade", "G4BinaryCascade", "G4Precompound" and "G4INCLCascade" as "G4BERTI", "G4BC", "G4PRECOM" and "G4INCL", respectively. Detailed descriptions and additional information of the above mentioned models are described well in the Physics Reference Manual [27] and Refs. [28, 29].

Recently, discrepancies between the experimental data and the simulation results obtained from hadronic models of GEANT4 in the low energy region were discussed in detail in Refs. [30, 31]. For more accurate simulations, data-based hadronic models for GEANT4 were developed by incorporating the Evaluated Nuclear Data File (ENDF/B-VII.1) [32]. The developed models were shown to have a good performance in those works [30, 31] and experimental verification of the model was also performed [33]. To see the validity of the ENDF/B-VII.1 data for ^{27}Al(p,n)^{27}Si reaction, we compare the results by the ENDF/B-VII.1 data with the experimental cross section data. Other nuclear data such as Japanese Evaluated Nuclear Data Library High Energy File 2007 (JENDL/HE-2007) [34], and TALYS-based evaluated nuclear data library (TENDL-2014) [35] can be available. Results by these nuclear data are also compared to the experimental data in this work.

^{27}Si with $T_{1/2}$ of 4.16 s emits electron-neutrinos through radioactive decay processes such as β^+ decay and electron capture (EC). Radioactive decay processes for ^{27}Si and subsequent emitted electron-neutrino energy distributions are simulated by using "G4RadioactiveDecay" [36, 37] class based on the Evaluated Nuclear Structure Data File

(ENSDF) [38].

III. RESULTS

A. Benchmarking simulations with experimental data

We first calculate proton induced ^{27}Si production cross sections from ^{27}Al target by using the hadronic models of GEANT4 mentioned in Sec. II. The calculated results are compared with the experimental data taken from the EXFOR database [26]. Results by the nuclear data are also compared with the measured data.

Cross sections for ^{27}Al(p,n)^{27}Si reaction with respect to the incident proton energy (E_p) are plotted in Fig. 1. The comparison of the calculated cross sections obtained from hadronic models of GEANT4 with the experimental data is given in Fig. 1 (a), where none of the models can reproduce the experimental cross sections satisfactorily. All the hadronic models considered in this work underestimate the experimental cross sections in $E_p \lesssim 15$ MeV region. Discrepancies between the calculated values and the measured those increase as the incident proton energy decreases. These discrepancies can be understood if we consider its widespread usage in many different scientific fields. In general, hadronic models of GEANT4 have been developed and tested for wide use. None of the models is specialized for both particular reaction channels and low energy regions [30, 31].

Therefore, in Fig. 1 (b), we show the results by more realistic nuclear data and compare to the experimental EXFOR data. In the incident proton energy $E_p \lesssim 10$ MeV region, all the nuclear data reproduce well the experimental data with error bar. For 10 MeV $\leq E_p \leq$ 15 MeV, ENDF/B-VII.1 (TENDL-2014) underestimates the experimental data about $\sim 19.3\%$ ($\sim 20.7\%$), and JENDL/HE-2007 overestimates the data about $\sim 9.2\%$. A comparison of Fig. 1 (b) with Fig. 1 (a) demonstrates that the nuclear data model can give more reasonable results than those by hadronic models of GEANT4 in the $E_p \leq 15$ MeV region. Especially JENDL/HE-2007 data reproduce well the experimental data within the experimental error ($\sim 10\%$). Additional benchmark simulations for ^{27}Al(p,xn) and ^{27}Al(p,xα) reactions are also performed in this work. The results are presented in Appendix A, which shows a tendency similar to the results shown in Fig. 1, *i.e.* the hadronic models are inferior to the nuclear models at least in the present simulation.

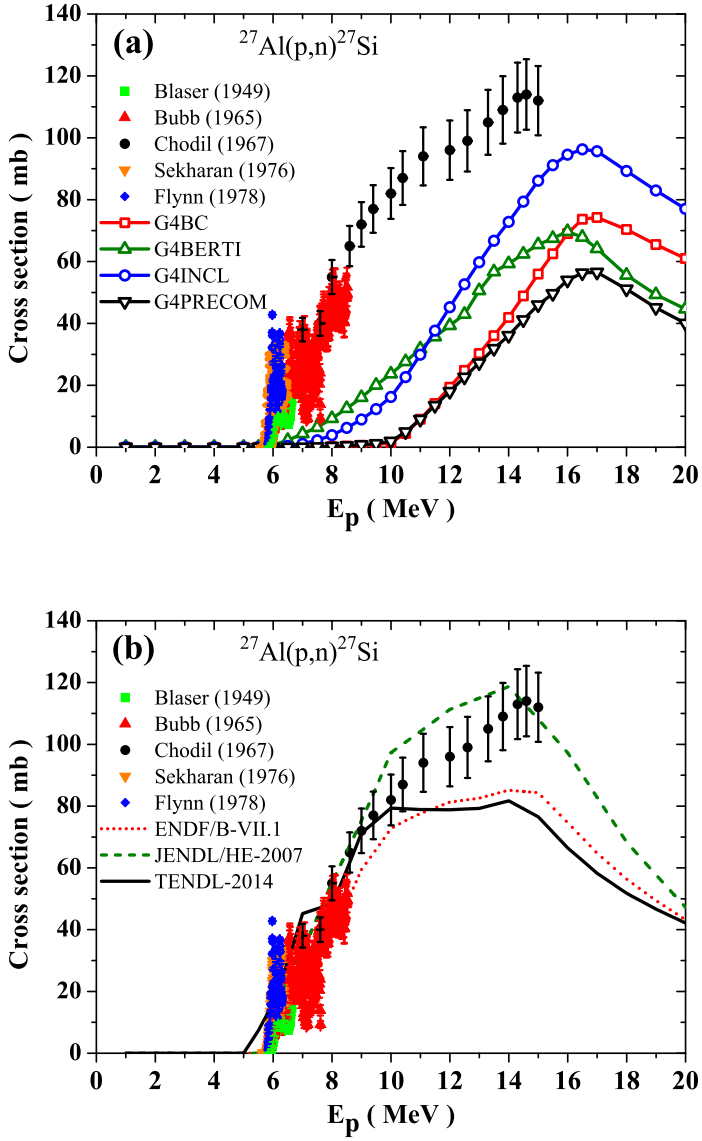

FIG. 1: (Color online) (p,n) reaction cross-sections on the ^{27}Al. The symbols denote various experimental data taken from the EXFOR database [26]. The experimental data are compared with the calculated cross sections using hadronic models of GEANT4 and nuclear data model in panel (a) and (b), respectively.

B. ^{27}Si yield calculation

Production of ^{27}Si through p + ^{27}Al reaction is considered in this study. Incident proton energy is chosen to be 15 MeV because of the following reasons. (1) There exist only limited

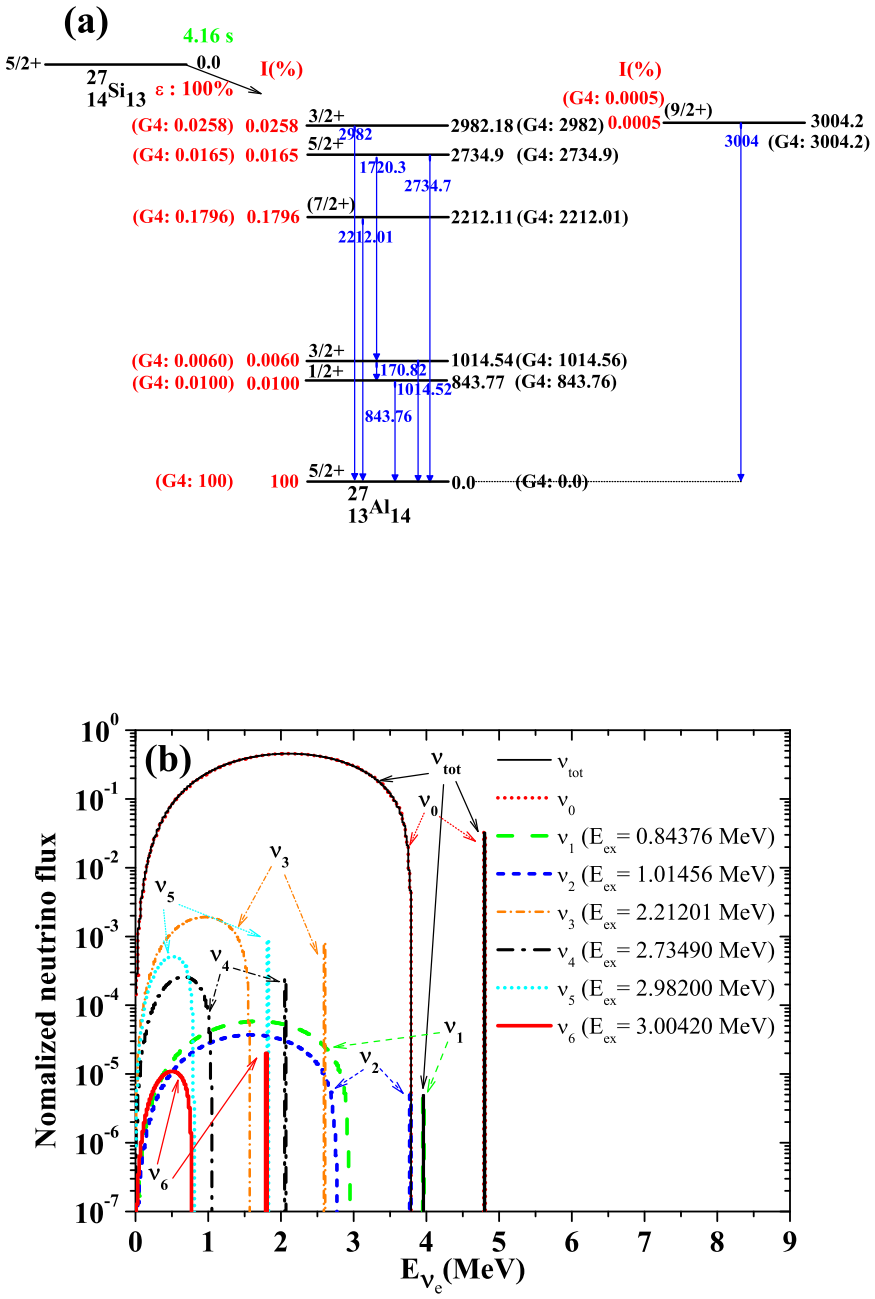

FIG. 2: (Color online) Upper panel (a) represents the energy levels (in the right hand side) and their decay scheme with the branching ratio (BR) (in the left hand side) of ^{27}Si. Values in parenthesis with G4 denote those used in GEANT4. Lower panel (b) notes the normalized energy distribution of electron-neutrinos through the decay of ^{27}Si. E_{ex} means the excitation level (MeV) of the daughter ^{27}Al reached after the decay. ν_0 means the electron-neutrinos with the residual ^{27}Al in the ground state. ν_1, ν_2, ν_3, ν_4, ν_5 and ν_6 denote the electron-neutrinos leaving the ^{27}Al with the excitation level 0.84376, 1.01456, 2.21201, 2.73490, 2.98200 and 3.00420 MeV, respectively. ν_{tot} is the sum from ν_0 up to ν_6. It should be noted that the large difference between ν_0 and others comes from the multiplied BRs in panel (a).

TABLE I: Numbers of ^{27}Si produced in ^{27}Al target in the units of [1/incident proton] $\times 10^{-4}$.

Physics Model	Number of ^{27}Si produced in the target [1/incident proton] $\times 10^{-4}$
JENDL/HE-2007	5.637 ± 0.289
TENDL-2014	4.435 ± 0.215
ENDF/B-VII.1	4.296 ± 0.175
G4PRECOM	0.981 ± 0.032

numbers of experimental data in the EXFOR database. Moreover, most of the data are centered in the energy region $E_p \lesssim 15$ MeV. For this reason, benchmark test of subsection III A for both the nuclear data and the hadronic models of GEANT4 is performed in this energy region. (2) By choosing this energy, we can suppress productions of unnecessary unstable isotopes which can make neutrino or anti-neutrino backgrounds through beta decays. For example, ^{23}Mg, ^{25}Al and ^{26}Si also produce electron-neutrino through beta decay processes. However, these isotopes are not generated in the present $E_p \lesssim 15$ MeV energy region, because threshold energies for ^{27}Al(p,n+α)^{23}Mg, ^{27}Al(p,t)^{25}Al and ^{27}Al(p,2n)^{26}Si reactions are 15.488 MeV, 16.536 MeV and 19.615 MeV, respectively. When the 15 MeV proton beam is used, ^{26}Al can be generated through ^{27}Al(p,d)^{26}Al (E_{th} = 11.237 MeV) or ^{27}Al(p,n+p)^{26}Al (E_{th} = 13.545 MeV) reactions. However, it has a very long life time of $\sim 10^5$ y. Also, ^{27}Al(p,2p)^{26}Mg (E_{th} = 8.580 MeV), ^{27}Al(p,p+α)^{23}Na (E_{th} = 10.468 MeV), ^{27}Al(p,α)^{24}Mg and ^{27}Al(p,γ)^{28}Si reactions are also possible, but the isotopes produced through the reactions are stable.

To calculate the production rate of ^{27}Si isotope, we use JENDL/HE-2007 and TENDL-2014 data as well as ENDF/B-VII.1 data for the simulations. Extracted nuclear data are converted into the GEANT4 format by using a TNudy (rooT NUclear Data librarY) program [39, 40] which is a nuclear data manipulation package based on the ROOT system [41]. The program can easily search, access and visualize the nuclear data relevant for user's specific purpose [39, 40]. Simulations with G4PRECOM are also performed for the comparison.

The ^{27}Al target is modeled as a cylinder of diameter 10 cm, whose thickness is chosen as 0.1 cm. The 1 cm thick ^{nat}C layer is placed behind the target for proton stopper. Numbers of ^{27}Si produced in ^{27}Al target are tabulated in Table I.

C. Energy spectra of electron-neutrinos from decay of ^{27}Si

Electron-neutrinos are emitted from ^{27}Si through β^+ decay and/or an electron capture (EC) process.

$$^{27}\mathrm{Si} \rightarrow {}^{27}\mathrm{Al} + e^+ + \nu_e, \tag{1}$$

$$^{27}\mathrm{Si} + e^- \rightarrow {}^{27}\mathrm{Al} + \nu_e. \tag{2}$$

For β^+ decay, a bound proton of ^{27}Si is changed into a neutron and an electron-neutrino is emitted from the parent nucleus with a positron in Eq. (1). The neutrinos generated by β^+ decay have continuous energy distributions. As a different type of radioactive decay, ^{27}Si can also be converted into ^{27}Al absorbing an inner shell electron (e.g. K-, L-, M-shell electrons), so-called EC or inverse β^+ decay in Eq. (2). During the process, the electron-neutrinos are produced with discrete energy due to two-body kinematics.

Decay and level schemes of ^{27}Si are drawn in Fig. 2 (a). Life time of ^{27}Si, branching ratios and excitation energies are based on the ENSDF data. The corresponding values used for GEANT4 simulations are also noted in parentheses. About 99.76% of ^{27}Si decay into a ground state of ^{27}Al, and the remaining $\sim$0.23% of ^{27}Si decay to one of six different excited states of ^{27}Al. During the decay process, ^{27}Si emits electron-neutrinos whose energies are restricted by each state of ^{27}Al.

Figure 2 (b) show the normalized neutrino energy spectra from decay of ^{27}Si. In this work, we simulate the decay of $10^9\times{}^{27}$Si, but all results are divided by 10^9. ν_0 means the electron-neutrinos with the residual ^{27}Al in the ground state. ν_1, ν_2, ν_3, ν_4, ν_5 and ν_6 denote the electron-neutrinos leaving the ^{27}Al with the excitation level 0.84376, 1.01456, 2.21201, 2.73490, 2.98200 and 3.00420 MeV, respectively. ν_{tot} is the sum from ν_0 up to ν_6, where the ν_0 contribution is dominant ($> 99.76\%$), while other contributions of $\nu_1 \sim \nu_6$ are marginal because of very small branching ratios.

In Fig. 2 (b), maximum monoenergy neutrino of 4.813 MeV in ν_0 as well as other monoenergies stem from the two body EC reaction, and continuous energy spectra come from the three body β^+ decay. Energy differences between the maximum energy of neutrino generated by β^+ decay and the discrete neutrino energy by EC are ~ 1.02 MeV. This feature can be understood by considering a sum of electron and positron masses in Eqs. (1) and (2).

Next monoenergy peak from ν_1 appears at $E_\nu = 3.97$ MeV in the figure, but it's intensity is much less than ν_0 due to EC by a factor of ~ 6500 because of the small branching ratio of the corresponding excited state shown in the panel (a) in Fig. 2. There is also a monoenergy peak of ν_2 at 3.799 MeV in Fig. 2 (b), but whose intensity is also very small like ν_1 from EC. As the excitation energy increases, neutrino energy spectra are shifted to lower energies. These shifts of the spectra are consistent with the difference between the excitation energies.

IV. DISCUSSION FOR ELECTRON-NEUTRINO DETECTION

In the previous sections, we proposed an accelerator based new artificial electron-neutrino source generated from decay of ^{27}Si for experiments of the vacuum-matter transition region. As noted in section III B, we produce a specific unstable isotope ^{27}Si in our case by choosing the 15 MeV proton beam. With the aid of the characteristics due to both an accelerator-based neutrino and a relatively short life time of ^{27}Si isotope (a few seconds), we can control an artificial neutrino beam, and thus remove background neutrinos for the detection in the following way. During the proton beam on ^{27}Al target, electron-neutrinos are generated from ^{27}Si. We can obtain signals ($S' = S_{s.} + S_{b.g.}$) in detecting-materials interacting with both the neutrinos from ^{27}Si ($S_{s.}$) and background neutrinos ($S_{b.g.}$). When the beam is switched off, on the other hand, the neutrinos are not produced. We can thus only obtain signals ($S = S_{b.g.}$) from the background. By subtracting the S from the S' we obtain the signal $S_{s.}$. Therefore, through the beam on and off, we may remove background neutrinos such as solar neutrinos, atmospheric neutrinos, geo-neutrinos, etc.

The expected electron-neutrino energy spectrum at a distance of 10 m from the ^{27}Al target is plotted in Fig. 3. The neutrinos are generated from decay of ^{27}Si produced by the 15 MeV and 10 mA proton beam on a ^{27}Al target. Although we assume the current of proton beam to 10 mA in this work, higher current beams from future's high power proton facilities can be available as reported in Refs. [42, 43]. The neutrino flux Φ_{ν_e} is evaluated by using GEANT4 with JENDL/HE-2007 data and G4RadioactiveDecay. Main contribution of the spectrum comes from the ν_0 through β^+ decay and the highest energy of ~ 4.813 MeV is emitted from the ν_0 by the EC, as explained in Fig. 2.

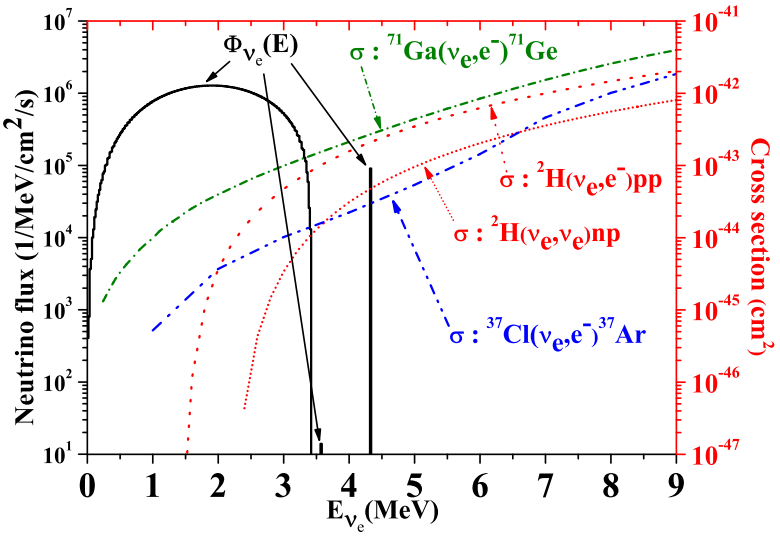

FIG. 3: (Color online) Generated neutrino spectrum. The black solid lines represent the expected electron-neutrino energy spectrum at a distance of 10 m from the ^{27}Al target. The neutrinos are generated from decay of ^{27}Si produced by the 15 MeV and 10 mA proton beam on a ^{27}Al target. For further discussions, we show theoretical cross section for ^{37}Cl(ν_e,e$^-$)^{37}Ar [44], ^{71}Ga(ν_e,e$^-$)^{71}Ge [45], ^{2}H(ν_e,e$^-$)pp [46] and ^{2}H(ν_e,ν_e)np reactions [46].

A. Radiochemical detectors

Here we discuss two different kinds of detections for the neutrino generated in the present simulation. One is the radiochemical detection technique, which has been widely used for the solar neutrino detection experiments. The cross sections for ^{37}Cl(ν_e,e$^-$)^{37}Ar [44], ^{71}Ga(ν_e,e$^-$)^{71}Ge [45], ^{2}H(ν_e,e$^-$)pp [46] and ^{2}H(ν_e,ν_e)np [46] reactions are plotted in Fig. 3 for the radiochemical detection of the neutrino from ^{27}Si.

The accelerator neutrino can be captured via the weak charged current reaction in the target nucleus such as ^{37}Cl and ^{71}Ga, and then new radioactive isotopes are produced. Those isotopes are chemically extracted and counted using their decay. Therefore, the neutrino source suggested in this work can be used for the calibration both ^{37}Cl and ^{71}Ga solar neutrino detector system.

Figure 4 shows the reaction rates calculated from the cross section in Fig. 3 with respect to the neutrino energy generated for a given condition. For both ^{37}Cl and ^{71}Ga, neutrinos

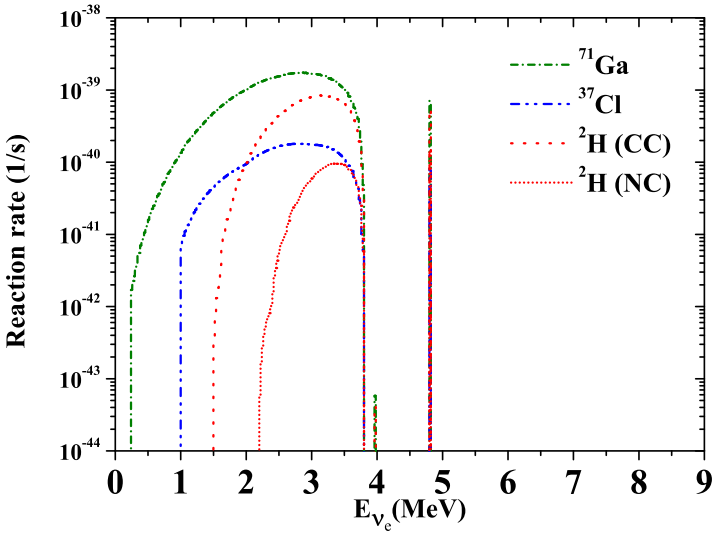

FIG. 4: (Color online) Electron-neutrino induced reaction rates via ^{37}Cl(ν_e,e$^-$)^{37}Ar, ^{71}Ga(ν_e,e$^-$)^{71}Ge, ^{2}H(ν_e,e$^-$)pp and ^{2}H(ν_e,ν_e)np reactions. The neutrinos are generated from decay of ^{27}Si which are produced by the 15 MeV and 10 mA proton beam on a ^{27}Al target. Results of the cross sections in Fig. 3 are exploited for this reaction rate calculation.

TABLE II: Radiochemical neutrino detector materials. The total reaction rates are calculated by both the electron-neutrino spectra obtained from this work and the cross sections mentioned in Fig. 3. The peak-to-total ratio in the 4th column means the ratio of the contribution from the ν_0 due to EC reaction to the total reaction rate.

Isotope	Reaction	Total reaction rate (1/s)	Peak-to-total ratio (%)
^{2}H	$\nu_e + {}^{2}\mathrm{H} \rightarrow e^- + \mathrm{p} + \mathrm{p}$	4.888E-38	1.127
	$\nu_e + {}^{2}\mathrm{H} \rightarrow \nu_e + \mathrm{p} + \mathrm{n}$	3.841E-39	3.790
^{37}Cl	$\nu_e + {}^{37}\mathrm{Cl} \rightarrow e^- + {}^{37}\mathrm{Ar}$	1.496E-38	0.579
^{71}Ga	$\nu_e + {}^{71}\mathrm{Ga} \rightarrow e^- + {}^{71}\mathrm{Ge}$	1.473E-37	0.478

having the continuous energy ($E_{th} < E_{\nu_e} <\sim 3.79$ MeV) and monoenergies (3.97 MeV and 4.813 MeV) interact with the isotopes. Contributions of the neutrino with two monoenergies of 3.97 MeV and 4.813 MeV are marginal. Their fractions in the total reaction rate of ^{71}Ga (^{37}Cl) turns out to be only 0.00004% (0.00004%) and 0.47809% (0.57929%) for 3.97 MeV and 4.813 MeV, respectively. Consequently, we can obtain the reaction rates or flux-averaged

cross sections for both ^{37}Cl(ν_e,e$^-$)^{37}Ar and ^{71}Ga(ν_e,e$^-$)^{71}Ge reactions in the neutrino energy region less than $\sim$ 3.79 MeV. This energy region is close to the vacuum-matter transition region in the solar neutrino physics.

One can see that widths of energy distributions of reaction rates for deuteron targets are more narrow than those for both ^{37}Cl and ^{71}Ga because of the reaction thresholds. With this feature, we can also have a chance to obtain reaction rates or energy averaged cross sections for ^{2}H(ν_e,e$^-$)pp and ^{2}H(ν_e,ν_e)np reactions with narrow neutrino energy region. Total reaction rates and the peak-to-ratio for reactions of the results in Fig. 4 are tabulated in Table II.

As another candidate of the radiochemical neutrino detection material, ^{127}I was also suggested in Ref. [47]. A first cross section measurement for ^{127}I(ν_e,e^-)^{127}Xe reaction was done by using the ν flux from the decay of stopped muons at the Los Alamos Meson Physics Facility (LAMPF) [48]. Their results are useful for super novae neutrino measurements because of the relatively high energy region of the neutrinos from LAMPF. But neutrino sources suggested in this work which have smaller energy range ($\sim<$ 3.79 MeV) than LAMPF can play an important role of improving the solar neutrino detection using ^{127}I.

B. Scintillator detectors

In addition, the neutrino source from this work can be useful for electron-neutrino detection studies with future's gigantic liquid-scintillator detectors (LSDs) such as LENA [49]. Through electron-neutrino electron (ν_e-e$^-$) elastic scattering (ES), neutrinos can be indirectly detected by the outgoing scattered electron, which electron can be identified by means of the scintillation light produced in the liquid scintillator. As a part of the European Large Apparatus for Grand Unification and Neutrino Astrophysics (LAGUNA) design study, the $\sim$ 50 kt LSD LENA (Low Energy Neutrino Astronomy) would have the feature of low detection threshold, good energy resolution, particle identification with efficient background discrimination [50–52].

With the electron-neutrino flux $\Phi_{\nu_e}(E_\nu)$ in Fig. 3, we obtain the expected reaction rate (R_{ν_e}) for LENA LSD. Differential reaction rate for the neutrinos from ^{27}Si can be obtained

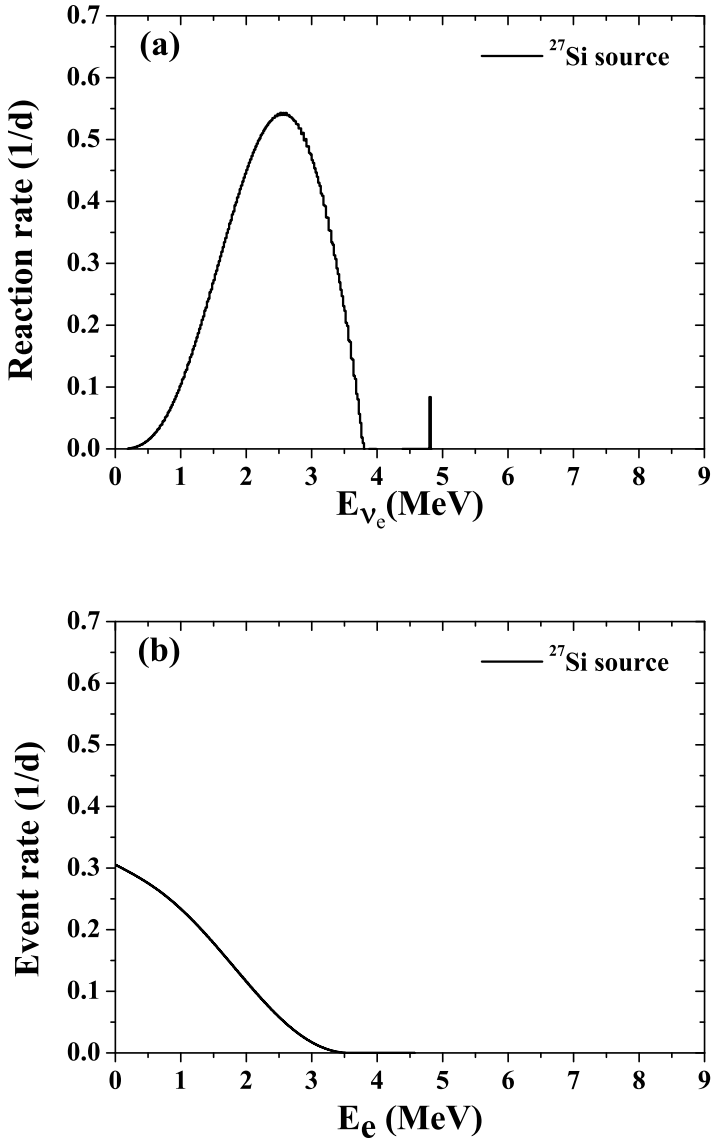

FIG. 5: (Color online) Panel (a) shows the reaction rate for electron-neutrino electron (ν_e-e$^-$) elastic scattering (ES) in the LENA detector. The neutrinos are generated from decay of ^{27}Si produced by the 15 MeV and 10 mA proton beams on a ^{27}Al target. The distance between the ^{27}Si source and the center of the LENA detector is assumed as 10 m. Panel (b) presents recoil energy distribution of the outgoing electron for the same condition.

by integrating over the neutrino energy [53]

$$\frac{dR_{\nu_e}}{dT} = n_e \int_0^{E_{max}} dE_\nu \Phi_{\nu_e}(E_\nu) \mathrm{P}_{ee}(E_\nu) \frac{d\sigma}{dT}. \tag{3}$$

where T is the kinetic energy of the recoil electron, n_e is the number of the electrons within the fiducial volume of LENA, $\Phi_{\nu_e}(E_\nu)$ is the electron-neutrino flux, E_{max} is the maximal neutrino energy, $\mathrm{P}_{ee}(E_\nu)$ is the energy dependent electron-neutrino survival probability, and E_ν is the energy of the incident neutrino. The $\frac{d\sigma}{dT}$ in Eq. (3) is the differential cross sections for neutrino-electron scattering which is give as [54]

$$\frac{d\sigma}{dT}(\nu_l e \to \nu_l e) = \frac{2G_\mu^2 m_e}{\pi E_\nu^2}[a^2 E_\nu^2 + b^2(E_\nu - T)^2 - abm_e T], \tag{4}$$

where G_μ is the Fermi constant, m_e is the mass of electron, and $a = -\frac{1}{2} - s^2$ and $b = -s^2$. The $s^2 = \sin^2\theta_W$ where θ_W is weak mixing angle. In our case, we use $\mathrm{P}_{ee}(E_\nu)$ given by [55]

$$P(\nu_e \to \nu_e) = 1 - \sin^2 2\theta_{13} S_{23} - c_{13}^4 \sin^2 2\theta_{12} S_{12}, \tag{5}$$

where $S_{23} = \sin^2(\Delta m_{32}^2 L/4E)$ and $S_{12} = \sin^2(\Delta m_{21}^2 L/4E)$.

Expected reaction rate for ν_e-e$^-$ ES is plotted in Fig. 5 (a). One can notice that dominant contribution of the reaction rate is the electron-neutrino with the energy range $\mathrm{E}_{th} < \mathrm{E}_{\nu_e} <\sim$ 3.79 MeV and sub-dominant contribution is the neutrino with a monoenergy 4.813 MeV. This feature can give us a chance to study for solar neutrino detections via ν_e-e$^-$ ES in the transition region between vacuum-dominated and matter-enhanced, where experimental understanding is still insufficient. Also, this may provide a test ground for the consistency of the standard model (SM), the determination of precision electroweak parameters, etc [54]. Total expected reaction rate is evaluated as 51.5392 count per day (cpd), and expected energy spectrum of recoil electron (event rate) via ν_e-e$^-$ ES is also plotted in Fig. 5 (b).

V. EFFECTS OF POSSIBLE STERILE NEUTRINOS

By using our neutrino source, we can also study the possibility of the existence of fourth neutrino, sterile neutrino. Electron-neutrino survival probabilities in the 3+1 and 3+2 scenarios can be written as [56]

$$P_{3+1} = 1 - 4|U_{e4}|^2(1 - |U_{e4}|^2)\sin^2(\Delta m_{41}^2 L/E), \tag{6}$$

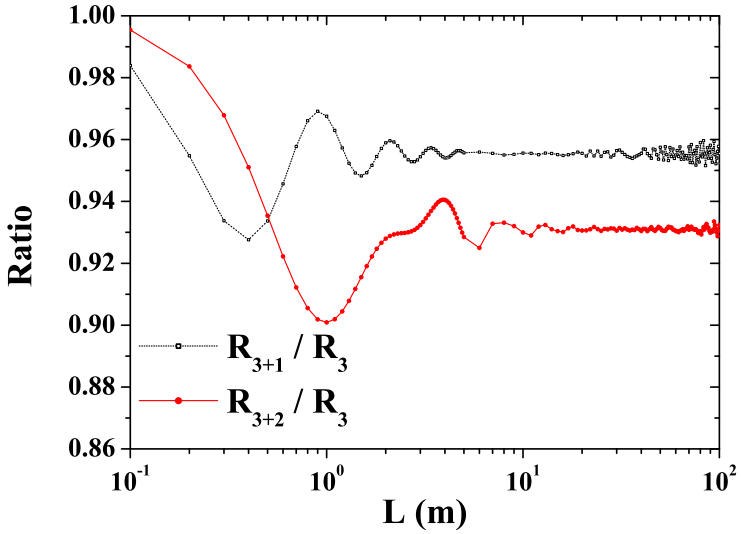

FIG. 6: (Color online) The ratio of the total reaction rate with P_{3+1} (or P_{3+2}) to the reaction rate with P_3 which is the same as P in Eq. (5). L means the distance between the ^{27}Si source and the center of the LENA detector.

$$\begin{aligned} P_{3+2} = 1 \; &- \; 4[(1-|U_{e4}|^2-|U_{e5}|^2) \\ &\times \; (|U_{e4}|^2 \sin^2(\Delta m^2_{41} L/E) \\ &+ \; |U_{e5}|^2 \sin^2(\Delta m^2_{51} L/E)) \\ &+ \; |U_{e4}|^2 |U_{e5}|^2 \sin^2(\Delta m^2_{54} L/E)]. \end{aligned} \tag{7}$$

The parameters in Eqs. (6) and (7) are taken from Ref. [57].

Figure 6 shows the ratio of the total reaction rate with P_{3+1} (or P_{3+2}) to the reaction rate with P_3 which is the same as P in Eq. (5). L is the distance between the ^{27}Si source and the center of the LENA detector. For L of a few ten's meters region, the value of R_{3+2}/R_3 is about 0.93. When L is chosen to 50 m, expected R_3, R_{3+1} and R_{3+2} are 2.06, 1.97 and 1.92 cpd, respectively. The R_{3+2}-to-R_3 ratio is 0.931, which is very close to the value of reactor experiments measured / expected rate = 0.927±0.023, so-called the short baseline reactor antineutrino anomaly [58, 59]. Therefore, together with an electron antineutrino disappearance search [56], our electron-neutrino source can be used for a precise measurement of the weak mixing angle at $\Delta m^2 \sim 1$ eV^2 relevant to the sterile neutrino.

Figure 7 (a) and (b) show possible effects by the sterile neutrinos on the expected reaction

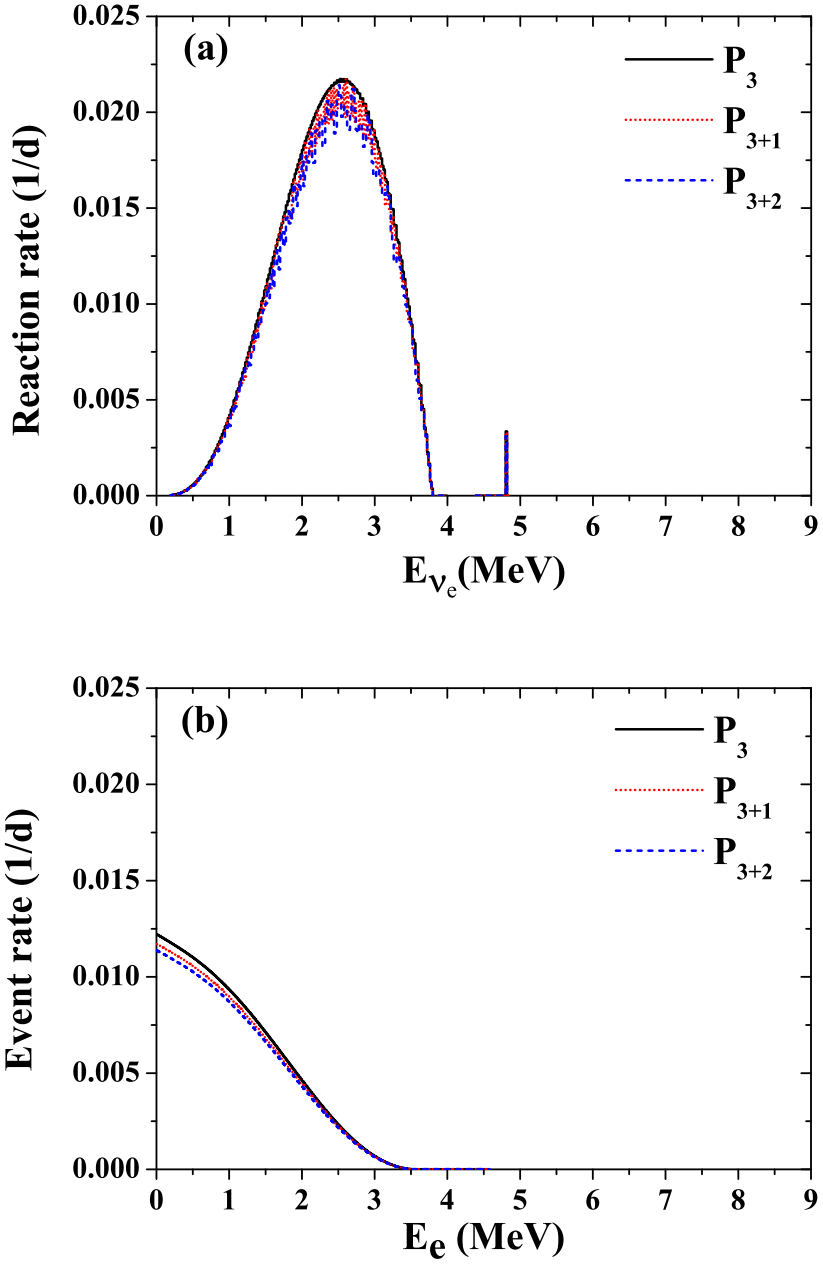

FIG. 7: (Color online) Effects of the sterile neutrinos on the reaction rate of ν_e-e$^-$ ES scattering, and recoiled energy distribution of the outgoing electron. Others are the same as Fig. 5. P_3, P_{3+1} and P_{3+2} are electron-neutrino survival probabilities in Eqs. (5), (6) and (7), respectively.

rate for ν_e-e$^-$ ES and the recoil electron energy spectra, respectively. The neutrino source and their physical conditions are the same as Fig. 5, but L is taken as 50 m in Fig. 7. The results of Fig. 7 are calculated with the P_3, P_{3+1} and P_{3+2} models, where P_3, P_{3+1} and P_{3+2} are electron-neutrino survival probabilities in Eqs. (5), (6) and (7), respectively.

As shown, in Figs. 6 and 7, sterile neutrinos would affect the reaction (event) rate, Eq. (3), 10% maximally, compared to the three active neutrino model. In particular, the 3+2 model influences the reaction much more than the 3+1 model. This feature would be a very interesting if the neutrino source is realized with reasonable detectors. Our suggestion may complement the simulation results regarding the effect of the sterile neutrinos on the disappearance of the antineutrino from the artificial ^{8}Li source in Ref. [56].

VI. SUMMARY

In this work, an artificial electron-neutrino source through ^{27}Al(p,n)^{27}Si reaction is investigated. The unstable isotope, ^{27}Si, produced by the reaction emits the electron-neutrinos via β^+ decay or electron capture (EC) process, whose energy regions are very close to the vacuum-matter transition region in the solar neutrino physics.

After extensive comparative study of the ^{27}Al(p,n)^{27}Si reaction with many nuclear data models, the JENDL/HE-2007 data turned out to reproduce well the experimental data within the experimental error ($\sim 10\%$), and thus ^{27}Si yields are evaluated by using GEANT4 with JENDL/HE-2007 data. Energy distributions of the electron-neutrino from ^{27}Si are obtained by using "G4RadioactiveDecay" class based on the Evaluated Nuclear Structure Data File (ENSDF). Neutrinos produced by the simulation are shown to have continuous energy spectra ($< \sim 3.79$ MeV) due to β^+ decay and discrete energy (4.81 MeV) caused by EC.

By using the electron-neutrino source confined in the neutrino energy region less than $\sim$ 3.79 MeV, we presented the reaction rates or flux-averaged cross sections for ^{37}Cl(ν_e,e$^-$)^{37}Ar and ^{71}Ga(ν_e,e$^-$)^{71}Ge as well as the deuteron target. The neutrino energy region produced in this work is located in the vacuum-matter transition region in solar neutrino physics, where experimental data for enough understanding are still insufficient.

In addition, we addressed that neutrino sources from this work can also be used for electron-neutrino oscillation studies with future's gigantic liquid-scintillator detectors (LSDs)

such as LENA. Possibility of detecting the sterile neutrino by using the electron-neutrino source and the LENA type detector is also discussed in detail. Our results are shown to enable us to properly disentangle the sterile neutrino mixing from the present electron-neutrino source.

Acknowledgments

The work of J. W. Shin is supported by the National Research Foundation of Korea (Grant No. NRF-2015R1C1A1A01054083), the work of M.-K. Cheoun is supported by the National Research Foundation of Korea (Grant No. NRF-2014R1A2A2A05003548).

Appendix A: Additional benchmark test for proton on ^{27}Al

For supplementary benchmarking tests, we also compared the simulated results by hadronic models of GEANT4 and nuclear data model with experimental cross sections for ^{27}Al(p,xn) and ^{27}Al(p,xα) reactions. As shown in Fig. 8 (a) and (c), all the hadronic models considered underestimate the experimental data, while the nuclear data model reproduces well the experimental cross section data.

[1] B. Pontecorvo, Sov. Phys. JETP **6**, 429 (1958), Available online at http://www.jetp.ac.ru/cgi-bin/e/index/e/6/2/p429?a=list .

[2] B. Pontecorvo, Zh. Eksp. Teor. Fiz. **33**, 549 (1958), Available online at http://www.jetp.ac.ru/cgi-bin/e/index/r/33/2/p549?a=list .

[3] B. Pontecorvo, Sov. Phys. JETP **7**, 172 (1958), Available online at http://www.jetp.ac.ru/cgi-bin/e/index/e/7/1/p172?a=list .

[4] B. Pontecorvo, Zh. Eksp. Teor. Fiz. **34**, 172 (1958), Available online at http://www.jetp.ac.ru/cgi-bin/e/index/r/34/1/p247?a=list .

[5] V. Gribov and B. Pontecorvo, Phys. Lett. B **28**, 493 (1969), http://dx.doi.org/10.1016/0370-2693(69)90525-5.

[6] R. Davis, D. S. Harmer, and K. C. Hoffman, Phys. Rev. Lett. **20**, 1205 (1968), http://dx.doi.org/10.1103/PhysRevLett.20.1205.

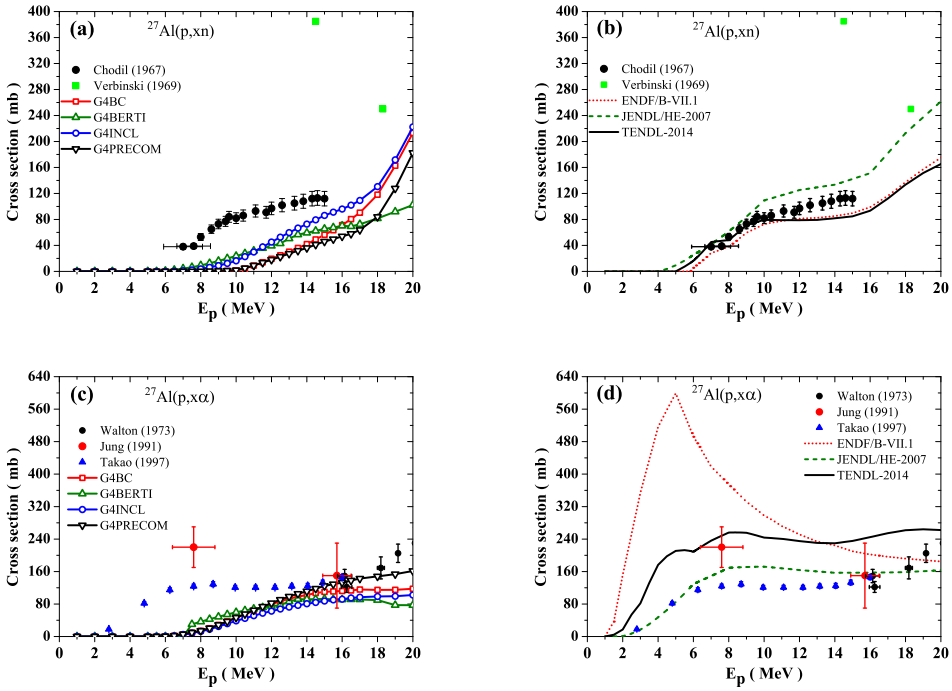

FIG. 8: (Color online) ^{27}Al(p,xn) reaction cross-sections are plotted in panel (a) by the hadronic model and panel (b) by the nuclear data model. (p,xα) reaction cross-sections for the ^{27}Al are presented in panel (c) and (d) by the hadronic and nuclear data model, respectively. See the caption of Fig 1. for the meaning of symbols and lines.

[7] K. Abe *et al.*, Phys. Rev. D **83**, 052010 (2011), http://dx.doi.org/10.1103/PhysRevD.83.052010.

[8] B. Aharmim *et al.*, Phys. Rev. C **88**, 025501 (2013), http://dx.doi.org/10.1103/PhysRevC.88.025501.

[9] G. Bellini *et al.*, Phys. Rev. Lett. **108**, 051302 (2012), http://dx.doi.org/10.1103/PhysRevLett.108.051302.

[10] L. Wolfenstein, Phys. Rev. D **17**, 2369 (1978), http://dx.doi.org/10.1103/PhysRevD.17.2369.

[11] L. Wolfenstein, Phys. Rev. D **20**, 2634 (1979), http://dx.doi.org/10.1103/PhysRevD.20.2634.

[12] S. P. Mikheyev and A. Y. Smirnov, Sov. J. Nucl. Phys. **42**, 913 (1985).

[13] S. P. Mikheyev and A. Y. Smirnov, Il Nuovo Cimento C **9**, 17 (1986), http://dx.doi.org/10.1007/BF02508049.

[14] G. Bellini, L. Ludhova, G. Ranucci, and F. L. Villante, Advances in High Energy Physics **2014**, 191960 (2014), http://dx.doi.org/10.1155/2014/191960.

[15] P. C. de Holanda and A. Y. Smirnov, Phys. Rev. D **69**, 113002 (2004), http://dx.doi.org/10.1103/PhysRevD.69.113002.

[16] P. C. de Holanda and A. Y. Smirnov, Phys. Rev. D **83**, 113011 (2011), http://dx.doi.org/10.1103/PhysRevD.83.113011.

[17] H. Minakata and C. Peña-Garay, Advances in High Energy Physics **2012**, 349686 (2012), http://dx.doi.org/10.1155/2012/349686.

[18] A. M. Serenelli, W. C. Haxton, and C. Peña-Garay, ApJ **743**, 24 (2011), http://dx.doi.org/10.1088/0004-637X/743/1/24.

[19] F. L. Villante, A. M. Serenelli, F. Delahaye, and M. H. Pinsonneault, ApJ **787**, 13 (2014), http://dx.doi.org/10.1088/0004-637X/787/1/13.

[20] S. Agostinelli *et al.*, Nucl. Instrum. Meth. A **506**, 250 (2003), http://dx.doi.org/10.1016/S0168-9002(03)01368-8.

[21] J. Allison *et al.*, IEEE Trans. Nucl. Sci. **53**, 270 (2006), http://dx.doi.org/10.1109/TNS.2006.869826.

[22] A. Heikkinen, N. Stepanov, and J. P. Wellisch, "Bertini intra-nuclear cascade implementation in Geant4," (2003), Computing in High Energy and Nuclear Physics 2003 Conference Proceedings, arXiv:nucl-th/0306008 .

[23] G. Folger, V. N. Ivanchenko, and J. P. Wellisch, Eur. Phys. J. A **21**, 407 (2004), http://dx.doi.org/10.1140/epja/i2003-10219-7.

[24] K. K. Gudima, S. G. Mashnik, and V. D. Toneev, Nucl. Phys. A **401**, 329 (1983), http://dx.doi.org/10.1016/0375-9474(83)90532-8.

[25] A. Boudard, J. Cugnon, J.-C. David, S. Leray, and D. Mancusi, Phys. Rev. C **87**, 014606 (2013), http://dx.doi.org/10.1103/PhysRevC.87.014606.

[26] "EXFOR database," (2015), Available online at `https://www-nds.iaea.org/exfor/exfor.htm` .

[27] "GEANT4 Physics Reference Manual," (2015), Available online at `http://geant4.web.cern.ch/geant4/support/index.shtml` .

[28] J. Apostolakis *et al.*, J. Phys.: Conf. Ser. **160**, 012073 (2009), XIII Int. Conf. on Calorimetry in High Energy Physics (CALOR 2008).

[29] J. Yarba, J. Phys.: Conf. Ser. **396**, 022060 (2012), Int. Conf. on Computing in High Energy and Nuclear Physics 2012 (CHEP2012).

[30] J. W. Shin and T.-S. Park, Nucl. Instrum. Meth. B **342**, 194 (2015), http://dx.doi.org/10.1016/j.nimb.2014.10.002.

[31] J. W. Shin, Nucl. Instrum. Meth. B **358**, 194 (2015), http://dx.doi.org/10.1016/j.nimb.2015.06.034.

[32] "ENDF/B-VII.1," (2015), Available online at `http://www.nndc.bnl.gov/csewg/` .

[33] J. W. Shin, S.-I. Bak, C. Ham, E. J. In, D. Y. Kim, K. J. Min, Y. Zhou, T.-S. Park, S.-W. Hong, and V. N. Bhoraskar, Nucl. Instrum. Meth. A **797**, 304 (2015), http://dx.doi.org/10.1016/j.nima.2015.06.042.

[34] "JENDL/HE-2007," (2015), Available online at `http://wwwndc.jaea.go.jp/index.html` .

[35] A. J. Koning and D. Rochman, Nuclear Data Sheets **113**, 2841 (2012), http://dx.doi.org/10.1016/j.nds.2012.11.002.

[36] P. Truscott, Tech. Rep. Qinetiq **60**, 2966 (2002).

[37] S. Hauf, M. Kuster, M. Batič, Z. W. Bell, D. H. H. Hoffmann, P. M. Lang, S. Neff, M. G. Pia, G. Weidenspointner, and A. Zoglauer, IEEE Trans. Nucl. Sci. **60**, 2966 (2013), http://dx.doi.org/10.1109/TNS.2013.2270894.

[38] "ENSDF," (2015), Available online at `http://www.nndc.bnl.gov/ensdf/` .

[39] S. I. Bak, R. Brun, F. Carminati, J. S. Chai, A. Gheata, M. Gheata, S.-W. Hong, Y. Kadi, V. Manchanda, T.-S. Park, and C. Tenreiro, J. Korean Phys. Soc. **59**, 1111 (2011), http://dx.doi.org/10.3938/jkps.59.1111.

[40] T.-S. Park, "TNudy project," (2015), unpublished.

[41] "Root," (2015), Available online at `https://root.cern.ch/` .

[42] N. V. Zamfir, Eur. Phys. J. Special Topics **223**, 1221 (2014), http://dx.doi.org/10.1140/epjst/e2014-02176-0.

[43] E. Akers, T. Satogata, S. Henderson, and V. R. Schaa, eds., *Proceedings of the 6th International Particle Accelerator Conference, Richmond, VA, USA, 3-8 May 2015* (2015) High power proton facilities: operational experience, challenges, and the future.

[44] J. N. Bahcall, E. Lisi, D. E. Alburger, L. D. Braeckeleer, S. J. Freedman, and J. Napolitano, Phys. Rev. C **54**, 411 (1996), http://dx.doi.org/10.1103/PhysRevC.54.411.

[45] J. N. Bahcall, Phys. Rev. C **56**, 3391 (1997), http://dx.doi.org/10.1103/PhysRevC.56.3391.

[46] S. Nakamura, T. Sato, S. Ando, T.-S. Park, F. Myhrer, V. Gudkov, and K. Kubodera, Nucl. Phys. A **707**, 561 (2002), http://dx.doi.org/10.1016/S0375-9474(02)00993-4.

[47] W. C. Haxton, Phys. Rev. Lett. **60**, 768 (1988), http://dx.doi.org/10.1103/PhysRevLett.60.768.

[48] J. R. Distel, B. T. Cleveland, K. Lande, C. K. Lee, P. S. Wildenhain, G. E. Allen, and R. L. Burman, Phys. Rev. C **68**, 054613 (2003), http://dx.doi.org/10.1103/PhysRevC.68.054613.

[49] M. Wurm *et al.*, Astropart. Phys. **35**, 685 (2012), http://dx.doi.org/10.1016/j.astropartphys.2012.02.011.

[50] R. Möllenberg, F. von Feilitzsch, D. Hellgartner, L. Oberauer, M. Tippmann, J. Winter, M. Wurm, and V. Zimmer, Phys. Lett. B **737**, 251 (2014), http://dx.doi.org/10.1016/j.physletb.2014.08.053.

[51] F. L. Villante, Phys. Lett. B **742**, 279 (2015), http://dx.doi.org/10.1016/j.physletb.2015.01.043.

[52] M. Wurm, D. Bick, T. Enqvist, D. Hellgartner, M. Kaiser, K. K. Loo, S. Lorenz, M. Meloni, M. Meyer, R. Möllenberg, L. Oberauer, M. Soiron, M. Smirnov, W. H. Trzaska, and B. Wonsak, Phys. Procedia **61**, 376 (2015), http://dx.doi.org/10.1016/j.phpro.2014.12.078.

[53] R. Möllenberg, *Monte Carlo study of solar* ^8B *neutrinos and the diffuse supernova neutrino background in LENA*, PhD dissertation, Technische Universitat, Munchen (2013), Available online at `http://mediatum.ub.tum.de/doc/1175550/file.pdf` .

[54] A. de Gouvêa and J. Jenkins, Phys. Rev. D **74**, 033004 (2006), http://dx.doi.org/10.1103/PhysRevD.74.033004.

[55] A. Strumia and F. Vissani, "Neutrino masses and mixings and ..." (2010), arXiv:hep-ph/0606054v3 .

[56] A. Bungau, A. Adelmann, J. R. Alonso, W. Barletta, R. Barlow, L. Bartoszek, L. Calabretta, A. Calanna, D. Campo, J. M. Conrad, Z. Djurcic, Y. Kamyshkov, M. H. Shaevitz, I. Shimizu, T. Smidt, J. Spitz, M. Wascko, L. A. Winslow, and J. J. Yang, Phys. Rev. Lett. **109**, 141802 (2012), http://dx.doi.org/10.1103/PhysRevLett.109.141802.

[57] J. Kopp, M. Maltoni, and T. Schwetz, Phys. Rev. Lett. **107**, 091801 (2011), http://dx.doi.org/10.1103/PhysRevLett.107.091801.

[58] G. Mention, M. Fechner, T. Lasserre, T. A. Mueller, D. Lhuillier, M. Cribier, and A. Letourneau, Phys. Rev. D **83**, 073006 (2011), http://dx.doi.org/10.1103/PhysRevD.83.073006.

[59] M. Cribier, J. Phys. Conf. Ser. **593**, 012005 (2015), http://dx.doi.org/10.1088/1742-6596/593/1/012005 .